

Article

# Optimization of Annealing Process of $\text{Li}_6\text{PS}_5\text{Cl}$ for All-Solid-State Lithium Batteries by Box–Behnken Design

Zhihua Zhang <sup>1</sup>, Yan Chai <sup>1</sup>, De Ning <sup>2</sup>, Jun Wang <sup>3</sup> , Dong Zhou <sup>4,\*</sup> and Yongli Li <sup>1,\*</sup> 

<sup>1</sup> Institute for Clean Energy Technology, North China Electric Power University, Beijing 102206, China; zhihua\_zhang@yeah.net (Z.Z.); yan.chai@ncepu.edu.cn (Y.C.)

<sup>2</sup> Centre for Photonics Information and Energy Materials, Shenzhen Institutes of Advanced Technology, Chinese Academy of Sciences, Shenzhen 518055, China; de.ning@siat.ac.cn

<sup>3</sup> School of Innovation and Entrepreneurship, Southern University of Science and Technology, Shenzhen 518055, China; wangj9@sustech.edu.cn

<sup>4</sup> Institute of Advanced Science Facilities, Shenzhen 518107, China

\* Correspondence: zhoudong@mail.iasf.ac.cn (D.Z.); yongli.li@ncepu.edu.cn (Y.L.)

**Abstract:**  $\text{Li}_6\text{PS}_5\text{Cl}$  possesses high ionic conductivity and excellent interfacial stability to electrodes and is known as a promising solid-state electrolyte material for all-solid-state batteries (ASSBs). However, the optimal annealing process of  $\text{Li}_6\text{PS}_5\text{Cl}$  has not been studied systematically. Here, a Box–Behnken design is used to investigate the interactions of the heating rate, annealing temperature, and duration of annealing process for  $\text{Li}_6\text{PS}_5\text{Cl}$  to optimize the ionic conductivity. The response surface methodology with regression analysis is employed for simulating the data obtained, and the optimized parameters are verified in practice. As a consequence,  $\text{Li}_6\text{PS}_5\text{Cl}$  delivers a rather high conductivity of 4.45 mS/cm at 25 °C, and ASSB consisting of a  $\text{LiNi}_{0.6}\text{Co}_{0.2}\text{Mn}_{0.2}\text{O}_2$  cathode and lithium anode shows a high initial discharge capacity of 151.7 mAh/g as well as excellent cycling performances for more than 350 cycles, highlighting the importance of the design of experiments.

**Keywords:** all-solid-state batteries;  $\text{Li}_6\text{PS}_5\text{Cl}$ ; Box–Behnken design; response surface methodology; ANOVA



**Citation:** Zhang, Z.; Chai, Y.; Ning, D.; Wang, J.; Zhou, D.; Li, Y.; Optimization of Annealing Process of  $\text{Li}_6\text{PS}_5\text{Cl}$  for All-Solid-State Lithium Batteries by Box–Behnken Design. *Batteries* **2023**, *9*, 480. <https://doi.org/10.3390/batteries9090480>

Academic Editor: Wilhelm Pflöging

Received: 13 August 2023

Revised: 29 August 2023

Accepted: 19 September 2023

Published: 21 September 2023



**Copyright:** © 2023 by the authors. Licensee MDPI, Basel, Switzerland. This article is an open access article distributed under the terms and conditions of the Creative Commons Attribution (CC BY) license (<https://creativecommons.org/licenses/by/4.0/>).

## 1. Introduction

The rising need for energy and pressing environmental issues have sparked worldwide attention towards advanced technologies. These technologies include electrified transportation and smart grids, which aim to efficiently store and utilize clean and renewable energy sources. Solar energy and its derivatives, such as wind, wave, and geothermal, are at the forefront of this sustainable energy movement. Secondary energy sources in chemistry, namely batteries, serve as the most crucial means of accommodating clean energy. They will play a pivotal role in achieving global carbon neutrality [1].

Contemporary commercial lithium-ion ( $\text{Li}^+$ ) batteries commonly employ combustible organic solvents as the electrolyte solution. Consequently, in order to mitigate the potential hazards associated with short circuits, it is imperative to incorporate safety mechanisms capable of restraining temperature elevation or enhancing the structural integrity and materials. In contrast, all-solid-state batteries (ASSBs) substitute the liquid electrolyte with a solid counterpart, thereby eliminating the necessity for combustible organic solvents within the battery system [2]. Additionally, the inclusion and recycling of Li metal, which possesses one of the lowest equivalent weights, allows for the attainment of minimal weights for anodes. This characteristic is particularly crucial for energy storage applications that require low weight per energy unit. However, in liquid electrolyte, the isolation of active Li masses from each other and from the current collector is a common drawback in the case of pure lithium deposition. Furthermore, the formation of shorts due to Li dendrites presents another failure mechanism in rechargeable Li-ion batteries, occasionally

resulting in battery explosions. In ASSBs, the aforementioned problem is likely to be solved by the solid physical properties of the solid electrolyte (SSE). As a result, ASSBs are anticipated to streamline safety measures while exhibiting remarkable performance in terms of manufacturing expenses and production efficiency [3].

Among various kinds of inorganic solid-state electrolytes (SSEs), sulfide SSEs, especially the argyrodites  $\text{Li}_6\text{PS}_5\text{Cl}$ , have drawn a lot of attention for their high Li-ion conductivity, stable  $\text{PS}_4^{3-}$  tetrahedral structure, compatible interface with oxide-based cathodes, abundant raw materials, and easy processability, which are critical requirements for the scalable fabrication of ASSBs [4–6].

Recently, various synthesis approaches of  $\text{Li}_6\text{PS}_5\text{Cl}$  have been reported [7]. Yu et al. prepared a  $\text{Li}_6\text{PS}_5\text{Cl}$  electrolyte with a conductivity of 1.62 mS/cm by ball milling at 550 rpm for 10 h followed by annealing at 550 °C for 5 h [8]. Zhang et al. prepared a  $\text{Li}_6\text{PS}_5\text{Cl}$  electrolyte with a high ionic conductivity of 1.8 mS/cm by ball milling at 600 rpm for 24 h followed by annealing at 600 °C at 0.3 °C/min [9]. Zhou et al. prepared a  $\text{Li}_6\text{PS}_5\text{Cl}$  electrolyte with a high ionic conductivity of 2.4 mS/cm by a solution approach and a subsequent annealing process under vacuum in a carbon-coated quartz tube [10]. Zhao et al. prepared a  $\text{Li}_6\text{PS}_5\text{Cl}$  electrolyte with a high ionic conductivity of 3.19 mS/cm by annealing the mixed precursors twice at 550 °C for 12 h [11]. However, from the above meaningful endeavors, it is noted that the optimal annealing process of  $\text{Li}_6\text{PS}_5\text{Cl}$  has not been studied systematically.

Design of experiments (DoE) is a systematically statistical tool, widely used in areas such as product design and process and quality improvement study. Common DoE designs include full factorial, orthogonal, mixture, Taguchi, and Box–Behnken design (BBD). They each identify influential factors and some interaction effects, determine all factor–result interactions, reduce the number of experiments, establish relationships between factors and results, find optimal factor combinations, and model variables and predict optimal conditions [12].

In this study, we optimize the ionic conductivity of  $\text{Li}_6\text{PS}_5\text{Cl}$  by investigating the interactions between the heating rate, annealing temperature, and duration of the annealing process using the most comprehensive method, i.e., BBD [12]. The response surface methodology (RSM) was utilized with regression analysis to simulate the obtained data, and the optimized parameters were validated through experimental testing. The results demonstrated that  $\text{Li}_6\text{PS}_5\text{Cl}$  exhibited a high conductivity of 4.45 mS/cm at 25 °C, and the ASSB, which included a cathode of  $\text{LiNi}_{0.6}\text{Co}_{0.2}\text{Mn}_{0.2}\text{O}_2$  and a lithium (Li) anode, displayed a high initial discharge capacity of 151.7 mAh/g and excellent cycling performance for over 350 cycles. These results underscore the significance of the design of experiments in optimizing the ionic conductivity of  $\text{Li}_6\text{PS}_5\text{Cl}$  SSEs.

## 2. Materials and Methods

### 2.1. Materials

$\text{Li}_2\text{S}$  (99.98%),  $\text{P}_2\text{S}_5$  (99%), and  $\text{LiCl}$  (99.0%) were purchased from Sigma-Aldrich without further purification.  $\text{LiNi}_{0.6}\text{Co}_{0.2}\text{Mn}_{0.2}\text{O}_2$  (NCM) cathode powder was obtained from commercial sources. Li foils with a thickness of 80  $\mu\text{m}$  were purchased from China Energy Lithium Co., Ltd., Tianjin, China. It should be noted that the appearance of the Li foil should be checked to ensure it is intact and free from obvious deformation or damage. At the same time, the cleanliness of the Li foil surface should be inspected. Use a clean brush to gently wipe the surface of the Li foil, remove the oxidation layer, and gently flatten it. All preparation processes were carried out in an argon-filled glove box with  $\text{H}_2\text{O} < 0.1$  ppm and  $\text{O}_2 < 0.1$  ppm (Lab Star, Mbraun, Germany) due to the oxygen- and moisture-sensitive nature of the raw materials.

### 2.2. Preparation of $\text{Li}_6\text{PS}_5\text{Cl}$ Precursor

$\text{Li}_2\text{S}$ ,  $\text{P}_2\text{S}_5$ , and  $\text{LiCl}$  were used as starting materials. Stoichiometric reagents based on  $\text{Li}_6\text{PS}_5\text{Cl}$  were ball-milled for 1 h at 500 rpm with a planetary ball mill apparatus

(Retsch PM400). The ball-milling step is crucial in achieving a homogenous distribution of the starting materials, promoting uniform chemical reactions. A total of 50 g  $\text{Li}_6\text{PS}_5\text{Cl}$  precursor mixture was prepared in one ball-milling jar for further use in the annealing process. A total of 50 g  $\text{Li}_6\text{PS}_5\text{Cl}$  precursor mixture was prepared in one ball-milling jar for further use in the annealing process. The purpose of synthesizing 50 g of precursor at one time is to increase the reproducibility of subsequent experiments. If the quantity of precursor is insufficient to meet the BBD experiments in the subsequent calcination process, it will result in inaccurate analysis of the experimental results.

### 2.3. Material Characterization

The crystalline phases of various samples were identified by collecting Powder X-ray Diffraction (XRD) patterns using  $\text{Cu K}\alpha$  X-rays (wavelength of 1.5406 Å at 45 kV and 40 mA) on a Bruker AXS D8 Advance diffractometer. In order to avoid any undesired reactions with moisture and oxygen, the powders were securely sealed within airtight XRD sample holders inside an argon-filled glove box. The scanning rate was set to 0.1 degree per minute. The GSAS II suite was utilized for Rietveld refinement. Sequential refinement was carried out for all phases, i.e.,  $\text{Li}_6\text{PS}_5\text{Cl}$ ,  $\text{Li}_2\text{S}$ ,  $\text{LiCl}$ , incorporating scale factor, zero-point, background, lattice parameters, phase fraction, fraction coordinates, occupancies, and thermal parameters. This enabled the determination of the major phase fraction and impurity fraction.

### 2.4. Cell Assembly

ASSBs were assembled by the cold pressing method. Initially, a solid electrolyte pellet was prepared by applying a pressure of 150 MPa to 130 mg of  $\text{Li}_6\text{PS}_5\text{Cl}$  powder. Subsequently, a cathode composite powder, weighing approximately 5 mg, was pressed onto the upper surface of the pellet at a pressure of 150 MPa. Following this, Li foil was affixed to the opposite side of the pellet as the anode, employing a pressure of 100 MPa. Finally, the resulting three-layered pellet was subjected to cold pressing at 150 MPa. Throughout these procedures, a nylon tube with a diameter of 10 mm served as the containment vessel, while stainless steel rods were employed as the current collectors. The cathode layer is a mixture of  $\text{Li}_6\text{PS}_5\text{Cl}$ , NCM powder, and vapor-grown carbon fiber in weight ratio of 30:69:1. No extra stacking pressure was used during cell cycling.

### 2.5. Electrochemical Measurements

The ionic conductivities ( $\sigma$ ) of the electrolytes were determined using the following formula:  $\sigma = L/RS$ , where L denotes the thickness, S represents the contact area between the solid-state electrolyte and the blocking electrode, and R signifies the resistance. The resistance of the electrolytes was assessed through electrochemical impedance spectroscopy (EIS) measurements employing a Solartron 1470E potentiostat electrochemical workstation. The EIS test was performed over a frequency range of 1 MHz to 10 mHz, with an amplitude of 10 mV. To serve as the blocking electrodes, carbon-coated aluminum foils were selected and affixed to both sides of the SSE pellets. A total of 250 mg of SSE powder was accurately weighed and compacted within a nylon tube ( $\phi$ 10 mm) under a pressure of 360 MPa, resulting in the formation of a densely packed pellet.

### 2.6. Response Surface Methodology

The RSM of ionic conductivity of  $\text{Li}_6\text{PS}_5\text{Cl}$  can be calculated by the following equation:  $\sigma = c_0 + c_1A + c_2B + c_3C + c_{12}AB + c_{13}AC + c_{23}BC + c_{11}A^2 + c_{22}B^2 + c_{33}C^2$ , where  $\sigma$  is the predicted ionic conductivity of  $\text{Li}_6\text{PS}_5\text{Cl}$  by utilizing this model; A, B, and C are the heating rate, annealing temperature, and duration of the annealing process, respectively. The constant term is denoted as  $c_0$ , while the coefficients of the linear terms are represented by  $c_i$  ( $i = 1, 2, 3$ ). The quadratic terms are characterized by the coefficients  $c_{ij}$  ( $i$  and  $j = 1, 2, 3$ ;  $i \neq j$ ), and the interaction factors are described by the coefficients  $c_{ii}$  (where  $i = 1, 2, 3$ ) [13].

### 3. Results

Figure 1a shows the synthesis process flow diagram of  $\text{Li}_6\text{PS}_5\text{Cl}$ .  $\text{Li}_2\text{S}$ ,  $\text{P}_2\text{S}_5$ , and  $\text{LiCl}$  were used as raw materials and ball-milled for 1 h at 500 rpm to obtain the  $\text{Li}_6\text{PS}_5\text{Cl}$  precursor. The mixture was subsequently subjected to the annealing process, following the BBD methodology illustrated in Figure 1b. This approach entails a combination of treatments positioned at the midpoint of the test space's edge and necessitates a minimum of three factors. The determination of the total number of experiments (N) required for a BBD design is expressed as  $N = 2x(x - 1) + c$ , where  $x$  represents the number of factors and  $c$  denotes the number of center points. For this particular investigation, three factors, each with three levels, and a total of five center points were designated, resulting in a total of 17 experiments ( $6 \times 2 + 5$ ). A, B, and C are assigned to the heating rate, annealing temperature, and duration of the annealing process, respectively. Compared to the conventional full factorial design in Figure 1c, which has a total number of experiments of 27 ( $3 \times 3 \times 3$ ), the BBD methodology offers a significant reduction in the number of experiments, thereby enhancing study efficiency and enabling the simultaneous consideration of multiple factors. Design Expert software (12.0.3.0, Stat-Ease Inc., Minneapolis, MN, USA) was utilized to design the experiment and measure the results [14].

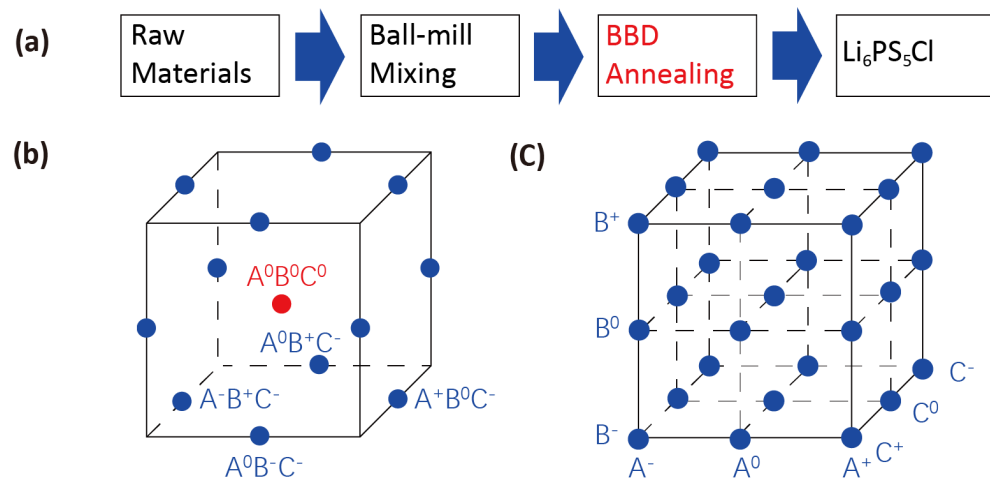


**Figure 1.** (a) The synthesis processes of  $\text{Li}_6\text{PS}_5\text{Cl}$ . (b) Schematic diagram of the BBD. (c) Schematic diagram of the full factorial design.

The experimental design of BBD is conducted by defining the real levels and coding levels for every parameter listed in Table 1, which encompasses the heating rate (A), annealing temperature (B), and annealing duration (C). The low, center, and high levels of each variable were denoted as  $-1$ ,  $0$ , and  $+1$ , respectively.

**Table 1.** The factors and levels in BBD for preparing  $\text{Li}_6\text{PS}_5\text{Cl}$ .

Parameters	Units	Factors	Coded Levels		
			$-1$	$0$	$1$
Heating rate	C/min	A	1	2	3
Temperature	$^{\circ}\text{C}$	B	540	550	560
Duration	min	C	180	240	300

After implementing the above experimental design, observed ionic conductivity values for each experiment were obtained, as presented in Table 2. Then, the statistical data were analyzed using the RSM method and the predicted ionic conductivity values can be calculated by the regression equation:  $\sigma = 4.262 + 0.0663A + 0.0188B + 0.2225C - 0.1400AB + 0.0625AC - 0.0925BC - 0.2310A^2 - 0.8610B^2 - 0.1435C^2$ .

**Table 2.** Comparative analysis of predicted and observed values in experimental runs of BBD.

Run	Factor 1	Factor 2	Factor 3	Actual Values	Predicted Values
	A: Heating rate °C/min	B: Temperature °C	C: Duration min	Conductivities S/cm	Conductivities S/cm
1	−1	0	−1	3.60	3.70
2	0	0	0	4.28	4.26
3	−1	0	1	3.93	3.98
4	0	0	0	4.32	4.26
5	0	0	0	4.18	4.26
6	−1	−1	0	3.02	2.93
7	0	1	−1	3.17	3.13
8	1	1	0	3.04	3.13
9	0	1	1	3.42	3.42
10	1	−1	0	3.32	3.38
11	0	−1	−1	2.91	2.91
12	0	−1	1	3.53	3.57
13	0	0	0	4.22	4.26
14	0	0	−1	3.72	3.67
15	−1	1	0	3.30	3.24
16	1	0	1	4.30	4.35
17	0	0	0	4.31	4.26

The experimental results presented in Figure 2a illustrate the ionic conductivity of  $\text{Li}_6\text{PS}_5\text{Cl}$ , as well as the predicted ionic conductivity obtained through regression analysis. It can be observed that all the experimental data align closely with the predicted values, suggesting that this regression model holds promise in predicting the ionic conductivity of  $\text{Li}_6\text{PS}_5\text{Cl}$  within the specified ranges of the three factors investigated [15]. However, it should be noted that the above conclusion only qualitatively indicates that Figure 2a helps to demonstrate the accuracy of the model, but it cannot determine the correctness of the accuracy through numerical values. The chart of the Box–Cox power transformation is shown in Figure 2b, where the optimal Lambda value is 0.03. This value is found by locating the minimum point of the curve generated by the natural logarithm of the sum of squared residuals, and its 95% confidence interval is  $-2.05$  to  $2.32$ , which includes 1 [16]. According to the definition of the use case of the Box–Cox power transformation, if the above situation occurs, the data do not need to undergo the Box–Cox power transformation, which indicates that the data points are indeed uniformly distributed on the line, thus proving the reliability of the model [17].

Furthermore, to evaluate the effectiveness of the parameters and the accuracy of the model, the analysis of variance (ANOVA), which can subdivide the total variation into some components related to the specific variance sources, is conducted, and the results are shown in Table 3.

Table 3 demonstrates the quality of the experimental data with the model using  $R^2$  (square of correlation coefficient), which is shown to be close to the desired value of 1.0 at 0.9899 [18]. The adjusted  $R^2$  value of 0.9768, which is a modified  $R^2$  value, demonstrates agreement with the predicted  $R^2$  of 0.8874 and falls within the normal limits [19]. Adeq Precision measures the signal-to-noise ratio, and the value of 22.3133 confirms an adequate signal, which is desirable for values greater than 4. Moreover, the model F value of 76.00 and  $p$ -value below 0.0001 indicate that the model is highly accurate and reliable, and there is only a 0.01% chance that an F value of this magnitude will occur due to the disturbance [20]. A  $p$ -value less than 0.0500 indicates that the model parameters are significant [21]. In this case, the linear effect of coefficients A and C, i.e., the heating rate ( $p$ -value of 0.0477) and duration ( $p < 0.0001$ ) are significant. Similarly, the interactive effects of the heating rate–temperature ( $p$ -value of 0.0090), and temperature–duration ( $p$ -value of 0.0499) are significant. Moreover, the  $p$ -values of the quadratic terms, i.e., the heating rate

(A2) ( $p$ -value of 0.0005), temperature (B2) ( $p < 0.0001$ ), and duration (C2) ( $p$ -value of 0.0070) are significant [21].

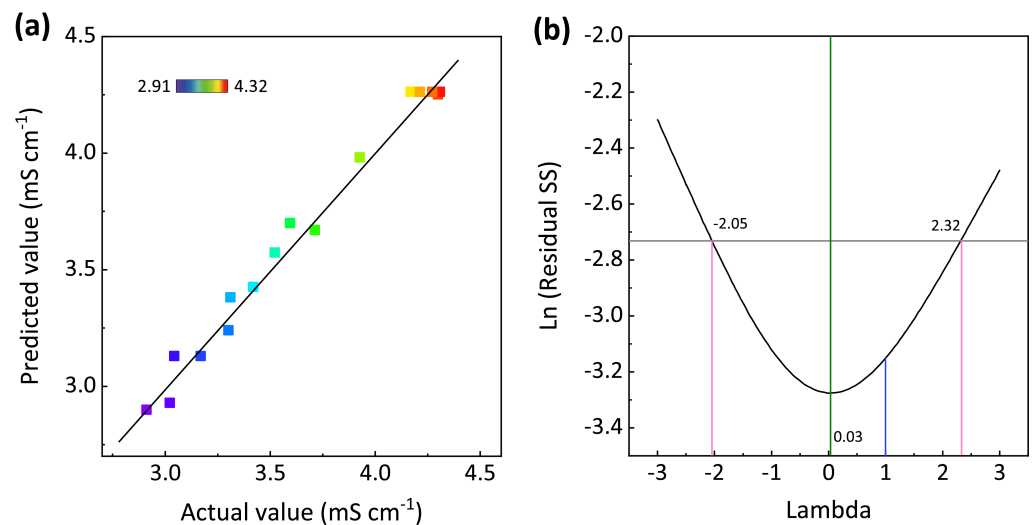


**Figure 2.** (a) The comparison between the actual and predicted ionic conductivity values of  $\text{Li}_6\text{PS}_5\text{Cl}$ . (b) Box–Cox plot for power transforms.

**Table 3.** ANOVA results of the ionic conductivity of  $\text{Li}_6\text{PS}_5\text{Cl}$  are conducted for each response.

Source	Sum of Squares	Degree of Freedom	Mean Square	F Value	$p$ -Value
Model	4.18	9	0.4647	76	<0.0001
A-Heating rate	0.0351	1	0.0351	5.74	0.0477
B-Temperature	0.0028	1	0.0028	0.4599	0.5194
C-Duration	0.396	1	0.396	64.77	<0.0001
AB	0.0784	1	0.0784	12.82	0.009
AC	0.0156	1	0.0156	2.56	0.154
BC	0.0342	1	0.0342	5.6	0.0499
$A^2$	0.2247	1	0.2247	36.74	0.0005
$B^2$	3.12	1	3.12	510.44	<0.0001
$C^2$	0.00867	1	0.00867	14.18	0.007
Residual	0.0428	7	0.0061		
Lack of Fit	0.0283	3	0.0094	2.61	0.1886
Pure Error	0.0145	4	0.0036		
Cor Total	4.23	16			

Quality of fitted to experimental data:  $R^2 = 0.9899$ , Adjusted  $R^2 = 0.9768$ , Predicted  $R^2 = 0.8874$ , Adeq Precision = 22.3133, CV = 2.12%.

In Figure 3, the contour plot and 3D response surface depict the relationship between the heating rate, temperature, and duration on the ionic conductivity of  $\text{Li}_6\text{PS}_5\text{Cl}$ . The influence of these variables on the ionic conductivity is evident in Figure 3a,b. As the annealing duration and temperature increase, the ionic conductivity initially rises and subsequently declines. Optimal levels of ionic conductivity are achieved when the annealing duration ranges from 270 to 300 min and the temperature ranges from 545 to 555 °C. Figure 3c,d demonstrate that both variables significantly impact the ionic conductivity of  $\text{Li}_6\text{PS}_5\text{Cl}$ . Specifically, when the heating rate is approximately 2–3 °C/min and the annealing duration exceeds 300 min, the ionic conductivity reaches high levels. Furthermore, Figure 3e,f indicate that these two variables also affect the ionic conductivity, with the maximum value observed at a heating rate of approximately 2–2.5 °C/min and an annealing temperature of around 550 °C. As a consequence, for the optimization of the annealing process on the ionic conductivity of  $\text{Li}_6\text{PS}_5\text{Cl}$ , the calculated results are as follows: heating rate of 2.5 °C/min, annealing temperature of 549 °C, and annealing duration of 312 min. Under the above

predicted optimum conditions,  $\text{Li}_6\text{PS}_5\text{Cl}$  is prepared via the ball-milling route followed by the annealing process.

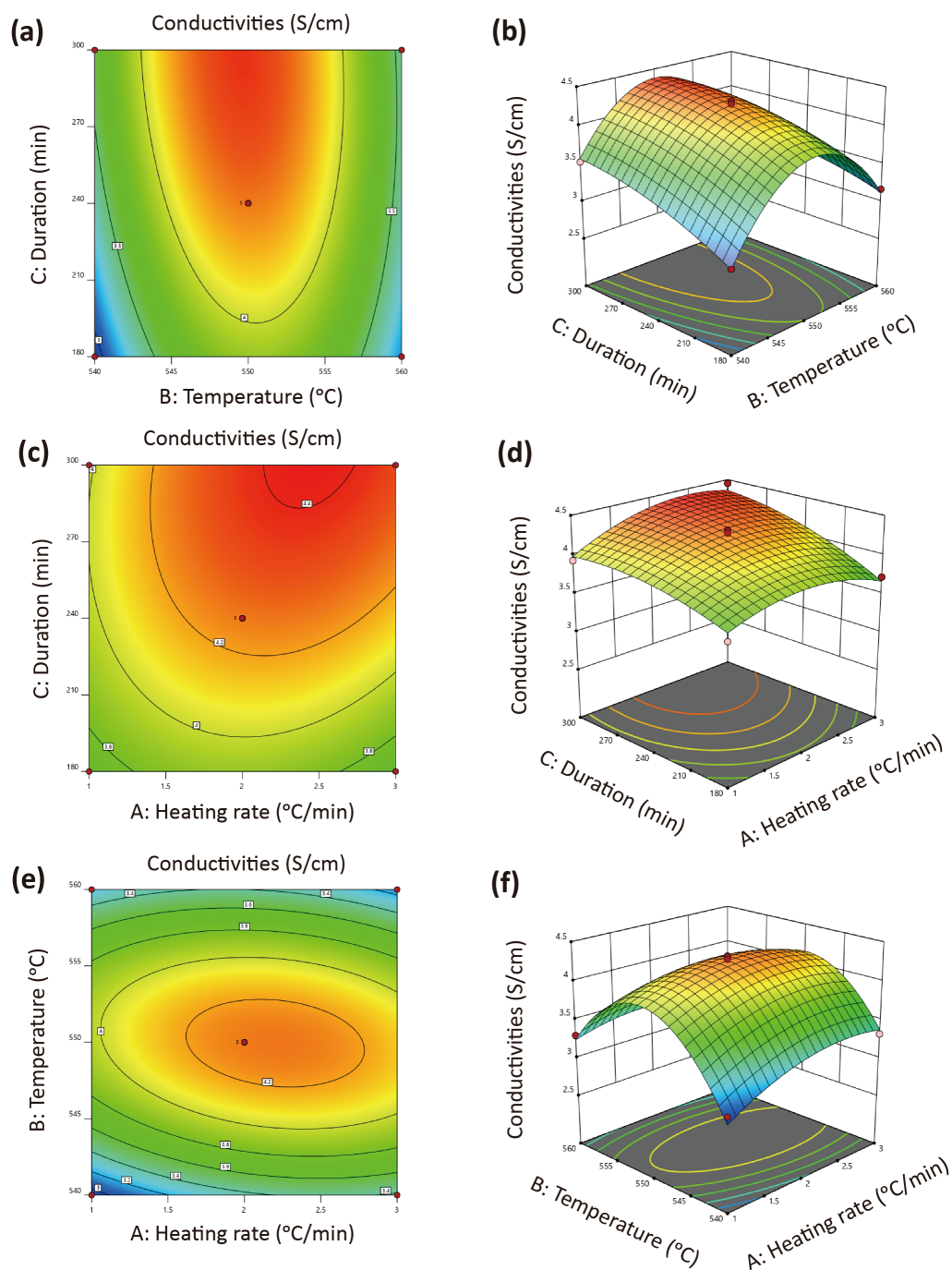


**Figure 3.** Contour plot and 3D response surface for effect of (a,b) the heating rate and temperature, (c,d) the heating rate and duration, and (e,f) the heating rate and temperature on the ionic conductivity of  $\text{Li}_6\text{PS}_5\text{Cl}$ .

Figure 4a shows the Nyquist plots and electronic conductivity test of the optimized  $\text{Li}_6\text{PS}_5\text{Cl}$ , which delivers an ionic conductivity of 4.45 mS/cm and an electronic conductivity of  $8.60 \times 10^{-5}$  mS/cm at 25 °C. Note that the  $\text{Li}_6\text{PS}_5\text{Cl}$  synthesized under optimum conditions exceeds that of the state-of-the-art  $\text{Li}_6\text{PS}_5\text{Cl}$  SSE reported in the recent literature, highlighting the significance of the BBD design of experiments [4,6,7,9,11,22]. In Figure 4b, the morphology of  $\text{Li}_6\text{PS}_5\text{Cl}$  particles is irregular, and particles are present where the size

of the primary particles is one to several micrometers; ref. [12] suggests that the parameters used during the heat treatment process do not induce anomalous particle growth.

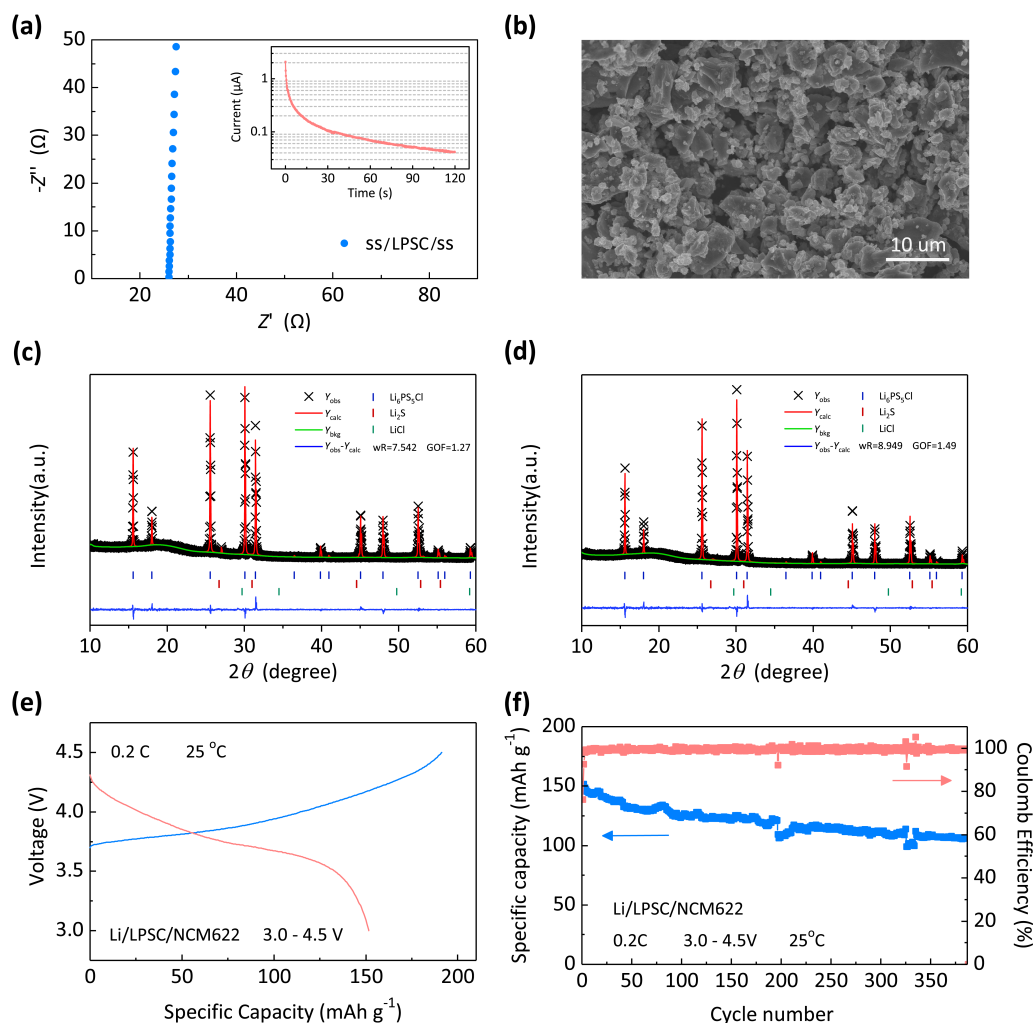


**Figure 4.** (a) Nyquist plots and electronic conductivity test, and (b) SEM of the  $\text{Li}_6\text{PS}_5\text{Cl}$  synthesized under the optimum annealing process. Rietveld refinement of XRD data for the pristine precursor mixture annealed under (c) condition 1 in Table 2 and (d) the optimum condition. (e) Charge–discharge curves and (f) cyclic performance of the NCM/Li ASSB using the optimized  $\text{Li}_6\text{PS}_5\text{Cl}$ .

To further investigate the higher conductivity led by the optimum condition, XRD data of the pristine precursor mixture annealed under the condition 1 in Table 2 or the optimum condition were refined using the Rietveld method implemented in GSAS II [23]. Figure 4c presents the diffraction pattern of the sample annealed under condition 1 in Table 2, with prominent peaks corresponding to the standard argyrodite phase of cubic  $\text{Li}_7\text{PS}_6$  (PDF34-0688) with a space group of  $F43m$  being evident. However, upon closer examination, it is apparent that at  $2\theta$  of  $27^\circ$ , diffraction peaks stemming from the  $\text{Li}_2\text{S}$  phases can be detected, indicating the presence of incomplete reactants [24]. Conversely, Figure 4d exhibits a diminished presence of reactant peaks from  $\text{Li}_2\text{S}$  or  $\text{LiCl}$ , corresponding to the higher  $\text{Li}_6\text{PS}_5\text{Cl}$  phase fraction (98.32%) in the optimized sample, which is substantially greater than that of 91.17% calculated in the mixture annealed under the first condition listed in Table 2. The optimal experimental conditions lead to a greater amount of fast ion conducting phases through the BBD experimental design, contributing to the enhancement of the apparent ionic conductivity of the SSE [8].

Figure 4e illustrates the charge–discharge profiles of NCM/Li ASSBs tested at a current rate of 0.2 C and a temperature of  $25^\circ\text{C}$ . The active material NCM exhibits a mass loading

of approximately 5 mg/cm<sup>2</sup>. The initial discharge capacity registers at 151.7 mAh/g, accompanied by a Coulombic efficiency of 79.1%. This reduction in efficiency might be attributed to disconnections at the interface between the electrode and current collector or temporary discharge polarization resulting from SEI formation [25]. Subsequently, the discharge capacity gradually diminishes, yielding a reversible discharge capacity of 107.6 mAh/g by the 350th cycle, with a capacity retention of 70.8% (Figure 4f). It is worth noting that the ASSB demonstrates an average Coulombic efficiency of over 99.5% throughout the charge/discharge cycling, indicating highly reversible electrode reactions.

#### 4. Conclusions

In summary, we optimize the annealing process parameters of Li<sub>6</sub>PS<sub>5</sub>Cl by using a BBD experimental design. Under the optimum conditions, the ionic conductivity of the synthesized Li<sub>6</sub>PS<sub>5</sub>Cl material surpasses that of the state-of-the-art reports. The performance of full cells, utilizing NCM as the cathode material, displayed long-term stability during cycling, exhibiting a discharge specific capacity of 151.7 mAh/g. Moreover, these cells demonstrated a good capacity retention of 70.8% over the course of 350 cycles, while maintaining an average Coulombic efficiency exceeding 99.5%. This research not only establishes a promising design principle for the development of highly Li-ion-conductive solid-state electrolytes, but also paves the way for the advancement of next-generation high-energy ASSBs.

**Author Contributions:** Methodology, Z.Z.; software, D.N.; resources, D.Z. and Y.L.; writing—original draft preparation, Z.Z.; writing—review and editing, Y.C.; supervision, J.W.; funding acquisition, D.Z. and Y.L. All authors have read and agreed to the published version of the manuscript.

**Funding:** This research was funded by the Guangdong Province major talent introducing program (2021QN020687), National Key R&D Program of China (2022YFB4002002), National S&T Fundamental Resources Investigation Program of China (2022FY101302), National Natural Science Foundation of China (52202331, 51902321).

**Data Availability Statement:** Not applicable.

**Conflicts of Interest:** The authors declare no conflict of interest

#### References

1. Zhang, S.; Zhao, F.; Chen, J.; Fu, J.; Luo, J.; Alahakoon, S.H.; Chang, L.Y.; Feng, R.; Shakouri, M.; Liang, J.; et al. A family of oxychloride amorphous solid electrolytes for long-cycling all-solid-state lithium batteries. *Nat. Commun.* **2023**, *14*, 3780. [[CrossRef](#)] [[PubMed](#)]
2. Yin, Y.C.; Yang, J.T.; Luo, J.D.; Lu, G.X.; Huang, Z.; Wang, J.P.; Li, P.; Li, F.; Wu, Y.C.; Tian, T.; et al. A LaCl<sub>3</sub>-based lithium superionic conductor compatible with lithium metal. *Nature* **2023**, *616*, 77–83. [[CrossRef](#)] [[PubMed](#)]
3. Zhang, Z.; Wang, J.; Jin, Y.; Liu, G.; Yang, S.; Yao, X. Insights on lithium plating behavior in graphite-based all-solid-state lithium-ion batteries. *Energy Storage Mater.* **2023**, *54*, 845–853. [[CrossRef](#)]
4. Wu, Z.K.; Chen, S.Q.; Yu, C.; Wei, C.C.; Peng, L.F.; Wang, H.L.; Cheng, S.J.; Xie, J. Engineering high conductive Li<sub>7</sub>P<sub>2</sub>S<sub>8</sub>I via Cl-doping for all-solid-state Li-S batteries workable at different operating temperatures. *Chem. Eng. J.* **2008**, *10*, 142–149. [[CrossRef](#)]
5. Wu, Y.Q.; Zhou, K.; Ren, F.C.; Ha, Y.; Liang, Z.T.; Zheng, X.F.; Wang, Z.Y.; Yang, W.; Zhang, M.J.; Luo, M.Z.; et al. Highly reversible Li<sub>2</sub>RuO<sub>3</sub> cathodes in sulfide-based all solid-state lithium batteries. *Energy Environ. Sci.* **2022**, *15*, 3470–3482. [[CrossRef](#)]
6. Su, J.; Pasta, M.; Ning, Z.Y.; Gao, X.W.; Bruce, P.G.; Grovenor, C.R.M. Interfacial modification between argyrodite-type solid-state electrolytes and Li metal anodes using LiPON interlayers. *Energy Environ. Sci.* **2022**, *15*, 3805–3814. [[CrossRef](#)]
7. Yu, C.; Zhao, F.; Luo, J.; Zhang, L.; Sun, X. Recent development of lithium argyrodite solid-state electrolytes for solid-state batteries: Synthesis, structure, stability and dynamics. *Nano Energy* **2021**, *83*, 105858. [[CrossRef](#)]
8. Yu, C.; Li, Y.; Willans, M.; Zhao, Y.; Adair, K.R.; Zhao, F.; Li, W.; Deng, S.; Liang, J.; Banis, M.N.; et al. Superionic conductivity in lithium argyrodite solid-state electrolyte by controlled Cl-doping. *Nano Energy* **2020**, *69*, 104396. [[CrossRef](#)]
9. Zhang, Z.; Zhang, L.; Liu, Y.; Yu, C.; Yan, X.; Xu, B.; Wang, L.-M. Synthesis and characterization of argyrodite solid electrolytes for all-solid-state Li-ion batteries. *J. Alloys Compd.* **2018**, *747*, 227–235. [[CrossRef](#)]
10. Zhou, L.; Park, K.-H.; Sun, X.; Lalère, F.; Adermann, T.; Hartmann, P.; Nazar, L.F. Solvent-Engineered Design of Argyrodite Li<sub>6</sub>PS<sub>5</sub>X (X = Cl, Br, I) Solid Electrolytes with High Ionic Conductivity. *ACS Energy Lett.* **2018**, *4*, 265–270. [[CrossRef](#)]
11. Zhao, C.G.; Lyu, M.M.; Bi, C.J.; Huo, S.D.; Li, S.R.; Xue, W.D. Synthesis of high ionic conductivity Li<sub>6</sub>PS<sub>5</sub>Cl solid electrolyte by second sintering process. *Results Chem.* **2022**, *4*, 100468. [[CrossRef](#)]

12. Ferreira, S.L.C.; Bruns, R.E.; Ferreira, H.S.; Matos, G.D.; David, J.M.; Brandão, G.C.; da Silva, E.G.P.; Portugal, L.A.; dos Reis, P.S.; Souza, A.S.; et al. Box-Behnken design: An alternative for the optimization of analytical methods. *Anal. Chim. Acta* **2007**, *597*, 179–186. [[CrossRef](#)] [[PubMed](#)]
13. Pinto, D.; Vieira, E.F.; Peixoto, A.F.; Freire, C.; Freitas, V.; Costa, P.; Delerue-Matos, C.; Rodrigues, F. Optimizing the extraction of phenolic antioxidants from chestnut shells by subcritical water extraction using response surface methodology. *Food Chem.* **2021**, *334*, 127521. [[CrossRef](#)] [[PubMed](#)]
14. Hooda, A.; Nanda, A.; Jain, M.; Kumar, V.; Rathee, P. Optimization and evaluation of gastroretentive ranitidine HCl microspheres by using design expert software. *Int. J. Biol. Macromol.* **2012**, *51*, 691–700. [[CrossRef](#)] [[PubMed](#)]
15. Chaker, H.; Ameer, N.; Saidi-Bendahou, K.; Djennas, M.; Fourmentin, S. Modeling and Box-Behnken design optimization of photocatalytic parameters for efficient removal of dye by lanthanum-doped mesoporous TiO<sub>2</sub>. *J. Environ. Chem. Eng.* **2021**, *9*, 104584. [[CrossRef](#)]
16. Azizi, A.; Seyyed Alizade Ganji, S.M. Relative floatability as a criterion for evaluating the separation performance of phosphate from iron. *Int. J. Min. Sci. Technol.* **2017**, *27*, 451–458. [[CrossRef](#)]
17. Khusro, A.; Aarti, C.; Agastian, P. Microwave irradiation-based synthesis of anisotropic gold nanoplates using *Staphylococcus hominis* as reductant and its optimization for therapeutic applications. *J. Environ. Chem. Eng.* **2020**, *8*, 104526. [[CrossRef](#)]
18. Zhang, N.; Bénard, P.; Chahine, R.; Yang, T.; Xiao, J. Optimization of pressure swing adsorption for hydrogen purification based on Box-Behnken design method. *Int. J. Hydrogen Energy* **2021**, *46*, 5403–5417. [[CrossRef](#)]
19. Ghodrati, M.; Mousavi-Kamazani, M.; Bahrami, Z. Synthesis of superhydrophobic coatings based on silica nanostructure modified with organosilane compounds by sol–gel method for glass surfaces. *Sci. Rep.* **2023**, *13*, 548. [[CrossRef](#)]
20. Dwivedi, G.; Sharma, M.P. Application of Box–Behnken design in optimization of biodiesel yield from *Pongamia* oil and its stability analysis. *Fuel* **2015**, *145*, 256–262. [[CrossRef](#)]
21. Sharma, P.; Sahoo, B.B.; Said, Z.; Hadiyanto, H.; Nguyen, X.P.; Nižetić, S.; Huang, Z.; Hoang, A.T.; Li, C. Application of machine learning and Box-Behnken design in optimizing engine characteristics operated with a dual-fuel mode of algal biodiesel and waste-derived biogas. *Int. J. Hydrogen Energy* **2023**, *48*, 6738–6760. [[CrossRef](#)]
22. Rajagopal, R.; Subramanian, Y.; Jung, Y.J.; Kang, S.; Ryu, K.S. Rapid Synthesis of Highly Conductive Li<sub>6</sub>PS<sub>5</sub>Cl Argyrodite-Type Solid Electrolytes Using Pyridine Solvent. *ACS Appl. Energy Mater.* **2022**, *5*, 9266–9272. [[CrossRef](#)]
23. Zhou, S.; Pu, Y.; Zhang, X.; Shi, Y.; Gao, Z.; Feng, Y.; Shen, G.; Wang, X.; Wang, D. High energy density, temperature stable lead-free ceramics by introducing high entropy perovskite oxide. *Chem. Eng. J.* **2022**, *427*, 131684. [[CrossRef](#)]
24. Yu, C.; Ganapathy, S.; Hageman, J.; van Eijck, L.; van Eck, E.R.H.; Zhang, L.; Schwieter, T.; Basak, S.; Kelder, E.M.; Wagemaker, M. Facile Synthesis toward the Optimal Structure-Conductivity Characteristics of the Argyrodite Li<sub>6</sub>PS<sub>5</sub>Cl Solid-State Electrolyte. *ACS Appl. Mater. Int.* **2018**, *10*, 33296–33306. [[CrossRef](#)] [[PubMed](#)]
25. Randau, S.; Walther, F.; Neumann, A.; Schneider, Y.; Negi, R.S.; Mogwitz, B.; Sann, J.; Becker-Steinberger, K.; Danner, T.; Hein, S.; et al. On the Additive Microstructure in Composite Cathodes and Alumina-Coated Carbon Microwires for Improved All-Solid-State Batteries. *J. Abbr.* **2021**, *33*, 1380–1393. [[CrossRef](#)]

**Disclaimer/Publisher’s Note:** The statements, opinions and data contained in all publications are solely those of the individual author(s) and contributor(s) and not of MDPI and/or the editor(s). MDPI and/or the editor(s) disclaim responsibility for any injury to people or property resulting from any ideas, methods, instructions or products referred to in the content.